Computer predictions of three-dimensional particle trajectories in gas turbines

B. Kannapprakasam* and A. Brownt

Computational multiphase flow modeling is presented for particle trajectories in stator and rotor passages and through a stage of gas turbines. This is a three-dimensional analysis in which account is taken of the effects of variations of flow parameters due to design and environmental changes as well as particle properties. Good agreement was found between the predictions and observed data. The new information on particle trajectories resulting from the work described in this article is that (1) the angle of particle entry to a stage has a significant effect on the location of particle impact and (2) the effects of shear flow relative to a particle that give rise to lift and influence drag contribute to particle dynamics and hence erosion. The lift forces are of second-order importance.

Keywords: *turbomachines: particle trajectories*

Introduction

The use of alternative fuels in industrial gas turbines such as residual oil, heavy oil, or solid fuel, perhaps burned in a fluidized bed, has given rise to serious problems of fouling, corrosion, and erosion of blades. Particle separators, filters, and cyclones can remove a large percentage of the most damaging particles, but significant amounts of small particles, ranging from 1 μm to 40 μm, still enter the turbine. These particles erode the blade surfaces. For some aircraft, there is a growing need for low-altitude operation and takeoff and landing over dusty, unimproved land areas and deserts. This leads to the routine ingestion of sand and dust into the gas turbine engines causing particle impacts on blade surfaces resulting in erosion. Thus there is degradation of engine performance and reduction of time betwen engine overhauls and engine life. This necessitates an understanding of particle trajectories in gas turbines so as to estimate damage to critical components and to modify design to keep erosion to a minimum.

Morsi and Alexander[1] carried out a theoretical investigation of particle trajectories around an isolated airfoil in incompressible flow as a step toward understanding particle erosion in gas turbines. Their approach was classical two dimensional: transforming the velocity field around a cylinder in the Z plane to that around an isolated airfoil in the W plane. Three-dimensional particle trajectory calculations are necessary for any real understanding of erosion damage in gas turbines. Lord and Singh[2] considered the trajectories of individual particles through an axial turbine stage. They assumed the particle concentrations were low enough for there to be no modification of the gas flow due to the presence of particles. Although their particle trajectory calculation procedures were three dimensional, to save computer time, they considered only two-dimensional gas flow in the blade-to-blade stream surface of a blade channel. Fluid velocity distribution through a blade channel was determined using the streamline curvature cascade flow solution method of Bindon and Carmichael.[3] The particle equations of motion allowed for axes of rotation, but in their chosen examples only stator blade channels were considered. The fluid flow program also predicted boundary-layer development, but this was ignored in calculating particle trajectories. Typical particle trajectories from Lord and Singh are shown in Figure 1. In addition, they have been concerned with modeling engine conditions in cascade experiments and have shown that errors in calculated particle trajectories occur when scaling on Stokes and Mach numbers only.[4]

Abdel Azim and Rashed[5] investigated particle trajectories and their associated velocity history in centrifugal compressors. The difference between the work of Abdel Azim and Rashed and the work of Lord and Singh (apart form the obvious difference between centrifugal and axial flow) was that the former introduced rebound characteristics for their spherical particles, whereas the latter were interested in determining if their angular particles impacted with surfaces but not if they rebounded. Abdel Azim and Rashed used the rebound characteristics of Grant *et al.*[6] given by

Normal restitution coefficient

$$=0.993-1.76\beta_1+1.56\beta_1^2-0.49\beta_1^3 \quad (1)$$

Tangential restitution coefficient

$$=0.988-1.66\beta_1+2.11\beta_1^2-0.67\beta_1^3 \quad (2)$$

where β_1 is the relative impingement angle. In general, their study showed that the deviation of particle paths from the gas streamlines increases with increased particle mean diameter and material density; the former has greater effect.

Today, probably the most concentrated efforts in predicting three-dimensional particle trajectories in turbomachinery are being made at the University of Cincinnati under the direction of W. Tabakoff.[7-18] The work at Cincinnati is reviewed in Tabakoff and Hamed,[7] who concluded that the equations governing the motion of particles in gas flow fields must be used in the most general form applicable to either fixed or rotating frames of reference. Typical particle trajectories are shown in Figures 2, 3, and 4.

An extensive review of the bases for predicting gas-particle flows with particular reference to turbomachinery was carried out by Kannapprakasam and Brown.[19]

Particle trajectory calculation procedure

We have developed a computer program to determine particle trajectories for two- or three-dimensional geometries using a fourth-order Runge-Kutta method of solution in an axial turbine stage for incompressible or compressible steady state

* Vasavi College of Engineering, Hyberabad-500 031, India
† School of Mechanical, Materials and Civil Engineering, Royal Military College of Science, Shrivenham, Swindon, Wiltshire, SN6 8LA, United Kingdom
Received 27 October 1985 and accepted for publication 16 February 1987

0142-727X/87/030195-10$3.00

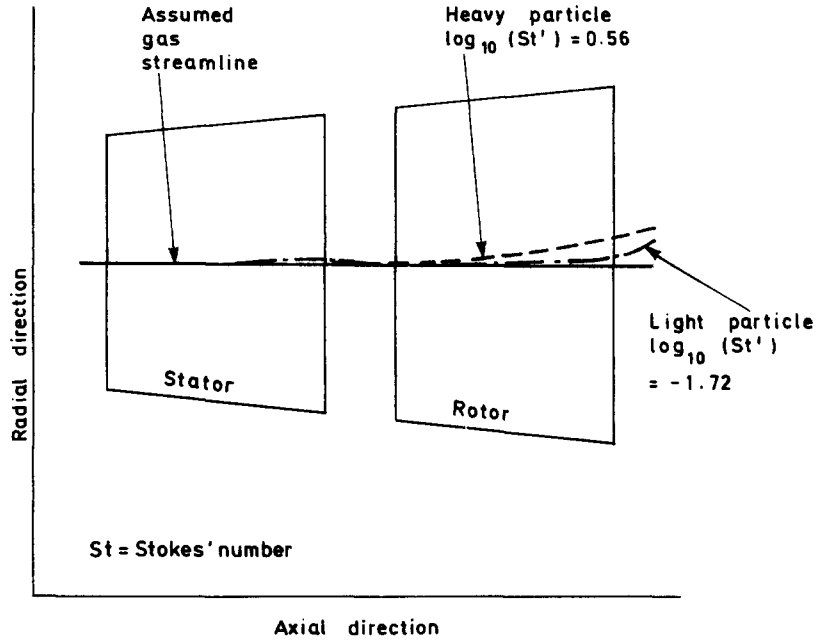

Figure 1 Particle trajectories in first stage of gas turbine (from Lord and Singh)

gas flows. For the gas flow analysis, we used the streamline curvature method of Katsanis[20] and modified by Vanco.[21] The input to the program is blade geometry, and the physical properties of particles and gas. The output includes streamline coordinates, gas velocity magnitude, and direction throughout the blade passages and the particle trajectory and velocities giving the locations of collision between the particle and blades and casing surfaces. Account is taken to particle dynamics including lift and spin and entry to the blade passage other than on a streamline. For these particle entries, any angle independent of the gas streamlines can be chosen. Any number of particles can be chosen across the pitch and span in the region upstream of the stator passage with equal or unequal spacing between the particles. The chosen blade profile is the same as that of Tabakoff and Hamed,[7] Hussein and Tabakoff,[12] and Beacher *et al.*[18]

In calculating particle trajectories, the equations of motion are integrated step by step using time steps. In general, the equations of motion of a particle in three dimensions are referred to an axis rotating at a given angular velocity, which for the case of a stator row, is chosen equal to zero. The equations of motion are:

$$\frac{dV_z}{dt}=\frac{18\mu_g F}{\rho_p d^2}(U_z-V_z)+EW_g^{3/2}\left(\frac{dV_r}{dr}\right)^{1/2} \tag{3}$$

$$\frac{dV_x}{dt}=\frac{18\mu_g F}{\rho_p d^2}(U_x-V_x)-\frac{V_r V_x}{r}-2\omega V_r \tag{4}$$

$$\frac{dV_r}{dt}=\frac{18\mu_g F}{\rho_p d^2}(U_r-V_r)+\omega^2 r+2\omega V_x+\frac{V_x^2}{r}+EW_g^{3/2}\left(\frac{dV_z}{dz}\right)^{1/2} \tag{5}$$

where the initial conditions are given by

$$\frac{dz}{dt}=W_{r0}\cos\theta_b \tag{6}$$

$$\frac{dx}{dt}=W_{r0}\sin\theta_b \tag{7}$$

$$\frac{dr}{dt}=W_{r0}\sin\theta_c \tag{8}$$

Notation

- c Axial projection of blade chord
- C_d Drag coefficient
- C_L Lift coefficient
- d Particle diameter
- d_{sr} Distance between stator and rotor
- F Correction factor for C_d at high Re
- E Lift parameter
- K Constant
- r Coordinate in radial (span) direction
- Re Reynolds number based on particle diameter and relative velocity
- s Span
- St Stokes number based on inlet gas velocity and axial projection of blade chord
- t Time
- U Fluid velcoity
- V Particle velocity
- W Particle velocity
- x Coordinate in circumferential direction
- z Coordinate in axial direction
- β Relative angle
- ψ Shape factor
- ω Angular velocity
- ρ Density
- $\bar{\rho}$ Ratio of particle to fluid density
- θ Angle of particle trajectory

Subscripts

- 0 Standard
- 1 Arriving (incident)
- 2 Leaving
- b Relative to axial and circumferential directions
- c Relative to axial and radial directions
- g Gas or relative
- p Particle
- r Relative to the radial direction
- $r0$ Initial
- x Relative to the circumferential direction
- z Relative to the axial direction

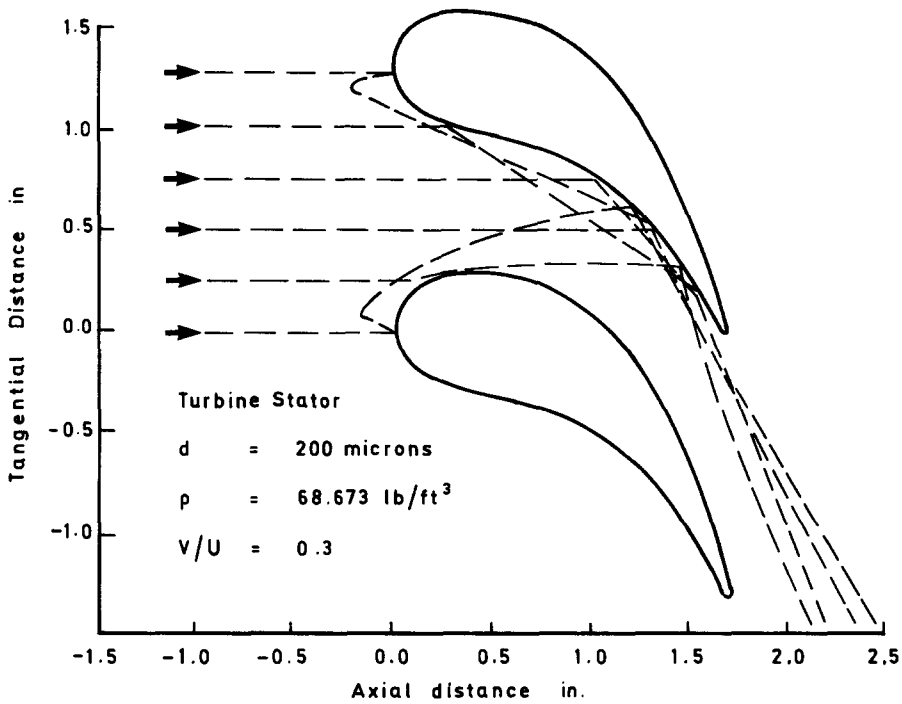

Figure 2 Example of particle trajectories through a turbine stator (from Takakoff and Hamed)

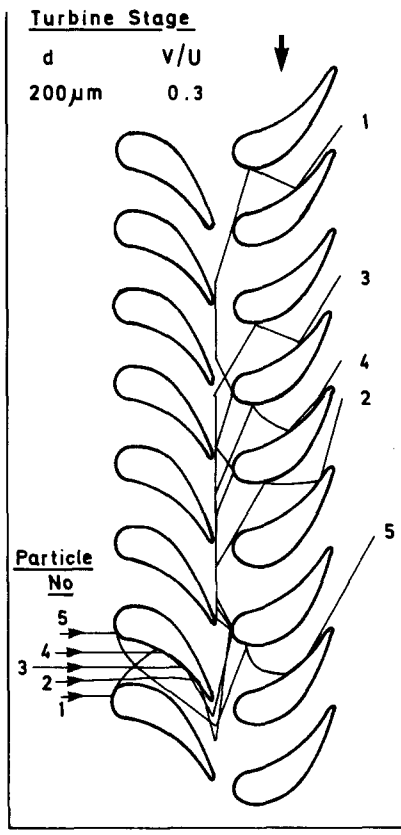

Figure 3 Example of particle trajectories relative to rotor blades (from Hussein and Tabakoff)

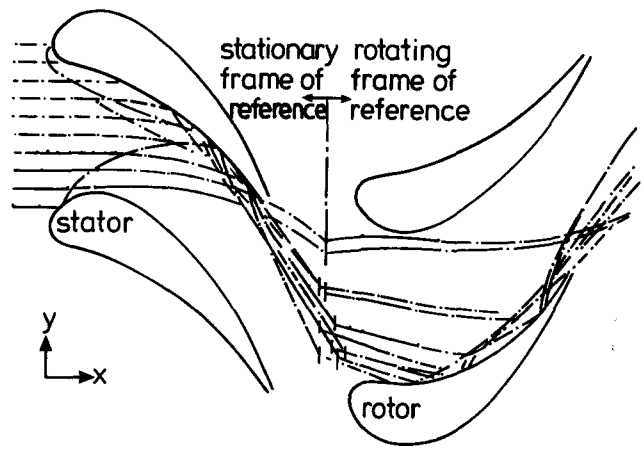

Figure 4 Calculated trajectories in particulate flow through turbine first stage (from Beacher *et al.*)

The three space coordinates are z, x, and r, where z is in the axial direction, x in the circumferential direction, and r in the span, that is, the radial direction, and t is time. The angle of a particle trajectory at entry to a turbine stage is θ_b relative to the blade surfaces and θ_c with respect to hub and casing. Fluid and particle velocities are U and V, respectively, and subscripts z, x, and r refer to the three coordinate directions. The initial particle velocity is W_{r0}, W_g is the particle relative velocity, and ω is the angular velocity of the rotor. Fluid viscosity is μ_g, particle density is ρ_p, and d is particle diameter. At high values of Re, F is the correction factor for C_d, where C_d is the drag coefficient of the fluid on the particle, and Re is Reynolds number based on particle diameter and relative velocity. From Tabakoff and Hamed,[7]

$$F = 1 = \frac{C_d \mathrm{Re}}{24} \quad \text{for } \mathrm{Re} < 1 \tag{9}$$

$$F = 1 + 0.188\,\mathrm{Re} = \frac{C_d \mathrm{Re}}{24} \quad \text{for } 1 < \mathrm{Re} < 4 \tag{10}$$

$$F = 0.914\,\mathrm{Re}^{0.282} + 0.0143\,\mathrm{Re} = \frac{C_d \mathrm{Re}}{24} \quad \text{for } 4 < \mathrm{Re} < 2000 \tag{11}$$

The lift parameter E is given by $E = 6\bar{\rho}(K + C_L)/\pi\psi d^{1/2}$, developed from the work of Saffman,[22] where:

$\bar{\rho}$ the ratio of particle to fluid densities
ψ the particle shape factor
C_L the coefficient of lift, and
K a constant usually taken to be unity.

These equations of motion include lift, and throughout the predictions presented in this article, we have assumed lift forces act radially outward only. Lift forces can be ignored by setting E equal to zero. We realize that lift forces from relative shear flows, including the effect of spin, act in more than the radial direction, but to save on computer time, we examined only one-dimensional lift. As we note later, the effect of lift forces on particle trajectories is of second-order importance. Equations 3, 4, and 5, subject to initial conditions expressed in Equations 6, 7, and 8, are solved simultaneously using a routine that incorporates features of the Runge-Kutta procedure. A typical example of the computer solution of the equations of motion for particle trajectories through a stator passage is shown in Figure 5, which compares favorably with those of Tabakoff and Hamed[7] shown in Figure 2. At the point of impact of particle with a solid surface, the rebound angle and velocity is determined from empirical restitution ratios, of which those due to Grant *et al.*[6] are typical.

$$\frac{\beta_2}{\beta_1} = 1 + 0.409\beta_1 - 2.52\beta_1^2 + 2.19\beta_1^3 - 0.531\beta_1^4 \tag{12}$$

and

$$\frac{V_2}{V_1} = 1 - 2.03\beta_1 + 3.32\beta_1^2 - 2.24\beta_1^3 - 0.472\beta_1^4 \tag{13}$$

where β_2/β_1 and V_2/V_1 are the ratios of angle of particle trajectory to surface and particle relative velocity leaving the surface to arriving at the surface, respectively. The particle trajectory calculations continue until the particle leaves the blade passage or until a specified computing time has elapsed. As a particle reaches a predetermined location downstream of a row of blades, the program calculates the new location for the next row of blades according to its frame of reference. In a stator row, the frame of reference is stationary, which is changed to a rotating frame of reference when entering a rotor row.

The location of impacts of particles on blade, hub, and casing surfaces and the impact and rebound angles and velocities are predicted by the computer program. Moreover, for a given concentration of particulates, the wear of surfaces over a given time can be determined. This has been done and will be reported later. Our main purpose in this article is to demonstrate the effects of geometric, environmental, and particle variations on particle trajectories through axial turbine stages.

Particle trajectories through axial turbine stages

To illustrate the effects of different particulate flow parameters on the dynamic behavior of particles, we consider three typical groups of parameters. The first group is the influence of design such as changing blade span, the axial distance between stator trailing edge and rotor leading edge, and the rotational speed of the rotor. The second group is environmental aspects such as particle size, density, and angularity and particle-to-gas velocity ratio at entry. The third group is particle–gas flow variations, which may be due to fluid properties such as change of particle trajectory entry angle and nonuniform distribution of particles in the entry plane to a row of blades. For comparison in demonstrating the calculation procedures, a standard blade-particle-gas combination has been defined, and the variations from the standard are stated on the appropriate figures when they occur. The standard is

Inlet gas temperature	$=1273°K$
Inlet gas density	$=1.225\ kg/m^3$
Shape factor	$=\psi=1.0$ (spherical)
Particle diameter	$=d=100\ \mu m$
Particle density	$=\rho_p=8000\ kg/m^3$
Ratio of particle to gas velocity at entry	$=V/U=0.15$
Angles of particle trajectory at entry	$=\theta_b=\theta_c=0$
Axial projection of blade chord for both stator and rotor	$=c=40$ mm
Rotor span	$=s=40$ mm
Stator and rotor pitch	$=40$ mm
Distance between stator trailing edge and rotor leading edge in the axial direction	$=d_{sr}=20$ mm
Rotor speed	$=\omega=24{,}000$ rpm
Number of stator and rotor passages	$=50$
Inlet gas velocity	$=U=25$ m/s
Lift ignored	$=E=0$

The variations from the standard for Figures 5 through 20 are listed in Table 1.

The maximum Reynolds number considered was 141, which gives a maximum value for F of 5.716 and a corresponding value for C_d of 0.971. The value of Stokes number for the standard situation at inlet was 57.0, which for a nonstandard particle of $d_p=10\ \mu m$ and $\rho_p=1112\ kg/m^3$ in the same gas and cascade conditions would reduce to 0.079. In presenting particle trajectory predictions in Figures 5 through 20, a maximum of three circumferential and three radial entry positions per stator passage are chosen, though many more have been examined.[2,3] Numbers in the figures refer to the number of the rotor row passage entered, assuming particles enter the stator row in passage number one. As the particles enter the stator row, the rotor instantaneously starts rotating at the chosen speed, and at this instant, it is further assumed the leading edges of number one stator and rotor blades are axially in line. The trajectories in stator passages are calculated in a stationary reference frame, and in rotor passages, a frame of reference moving at rotor speed is used. Between stator trailing edge and rotor leading, the centripetal acceleration due to rotor rotation can be assumed to start at any position between these two points. The numbers of gas data points in the gas passage between any two blades in a given row have maximum values of 50 in the radial and 50 in the circumferential directions and 100 in the through-flow direction, which is taken from midway between the trailing edge of the upstream row and the leading edge of the row of blades of interest to midway between its trailing edge and the leading edge of the downstream row. With maximum gas data points, the three-dimensional grid is fine enough to assume the gas properties relevant to a current particle position is that of the nearest gas grid node. When using less than the maximum gas data points, linear interpolation is used for particle positions not coincident with a gas data point.

Lift forces may occur on particles due to either particle spin or their shape and attitude characteristics. Lift is introduced to the calculation procedure via a nonzero value of the function E in Equations 3 and 5. Typical trajectories for $E \neq 0$ are shown in

Table 1 Variations from the standard for Figures 5–20

Figure	Variations		
5	Standard		
6	Standard		
7	$E \neq 0$		
8	$E \neq 0$		
9	$s/s_0=0.5$		
10	$s/s_0=2.0$		
11	$d_{sr}/d_{sr0}=2.0$		
12	$d_{sr}/d_{sr0}=0.5$	$\omega/\omega_0=0.25$[a]	
13	$d_{sr}/d_{sr0}=0.5$	$\omega/\omega_0=0.25$	$\rho_p/\rho_{p0}=0.139$
14	$d_{sr}/d_{sr0}=0.5$	$\omega/\omega_0=0.25$	$d/d_0=0.1$
15	$d_{sr}/d_{sr0}=0.5$	$\omega/\omega_0=0.25$	$\psi=0.75$
16	$d_{sr}/d_{sr0}=0.5$	$\omega/\omega_0=0.25$	$(V/U)/(V/U)_0=4$
17	$d_{sr}/d_{sr0}=0.5$	$\omega/\omega_0=0.25$	$\theta_b=\theta_c=45°$
18	$d_{sr}/d_{sr0}=0.5$	$\omega/\omega_0=0.25$	$\theta_b=\theta_c=45°$
19	$d_{sr}/d_{sr0}=0.5$	$\omega/\omega_0=0.25$	$\theta_b=\theta_c=-45°$
20	$d_{sr}/d_{sr0}=0.5$	$\omega/\omega_0=0.25$	$\theta_b=\theta_c=-45°$

[a] Subscript 0 = standard.

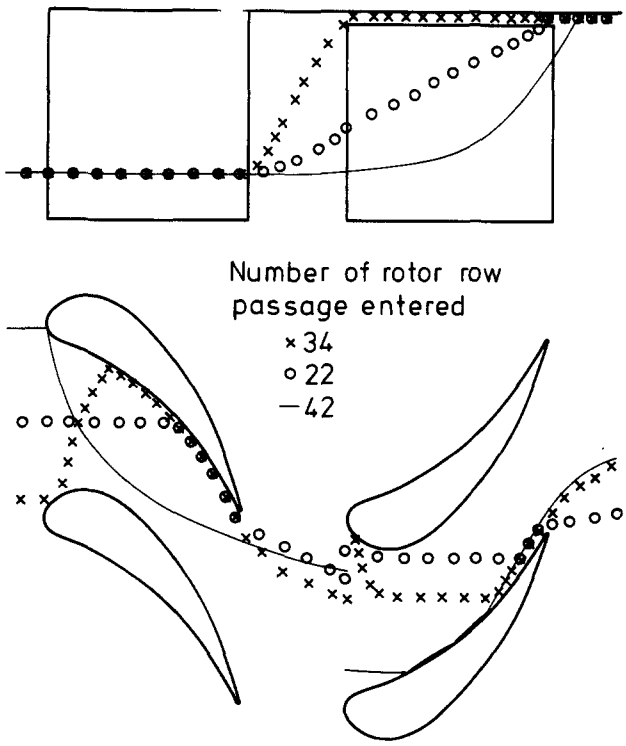

Figure 5 Particle trajectories for standard geometric, flow, and particle properties

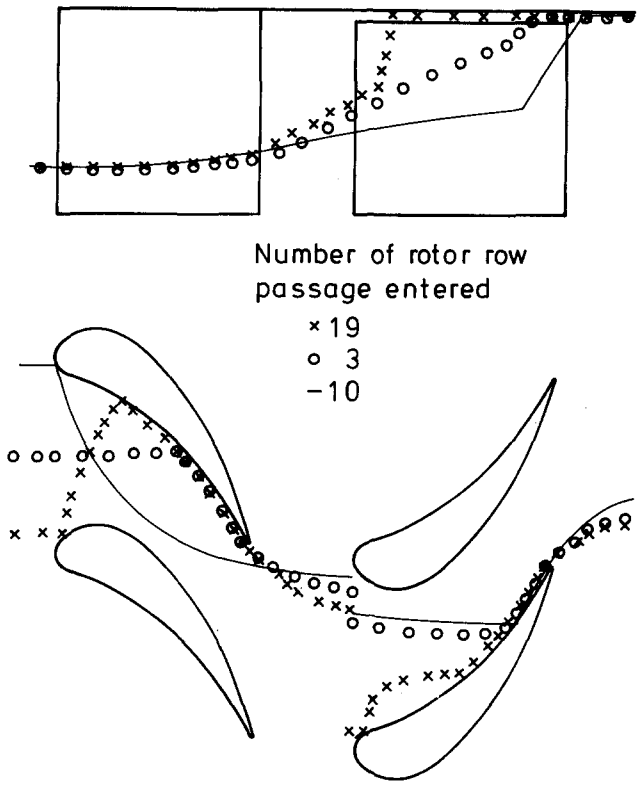

Figure 7 Particle trajectories for nonstandard geometric, flow, and particle properties, $E \neq 0$ (see Table 1)

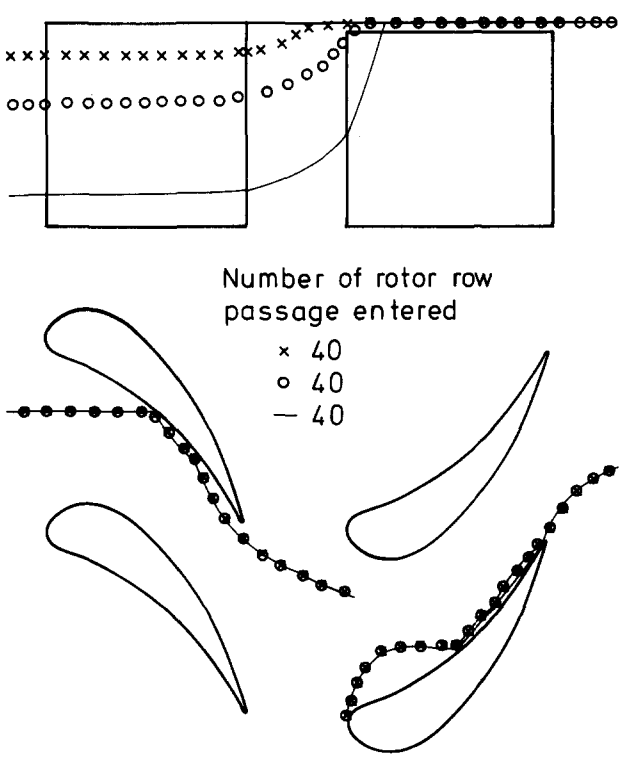

Figure 6 Particle trajectories for standard geometric, flow, and particle properties

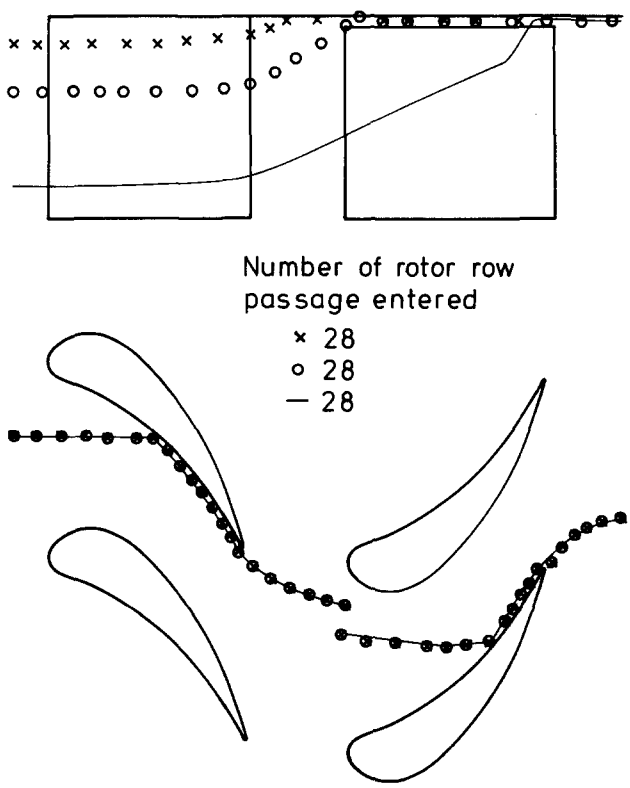

Figure 8 Particle trajectories for nonstandard geometric, flow, and particle properties, $E \neq 0$ (see Table 1)

Figures 7 and 8, which are to be compared with Figures 5 and 6 for $E = 0$. Unidirectional lift has been assumed, but in practice, it could occur in three-dimensions. In Figures 7 and 8, it can be seen that particles begin to move radially outward in the stator passage and thus have flight times different from previously in arriving at rotor entry. Differences therefore occur in the number of the rotor passage entered and surface positions impacted. Examining the effect of lift over a wide range of particle-fluid-geometry variations, we concluded particles reach the casing slightly earlier when radial lift forces are present. The extent and location of impact regions on blade surfaces are marginally different when life forces are taken into account; that

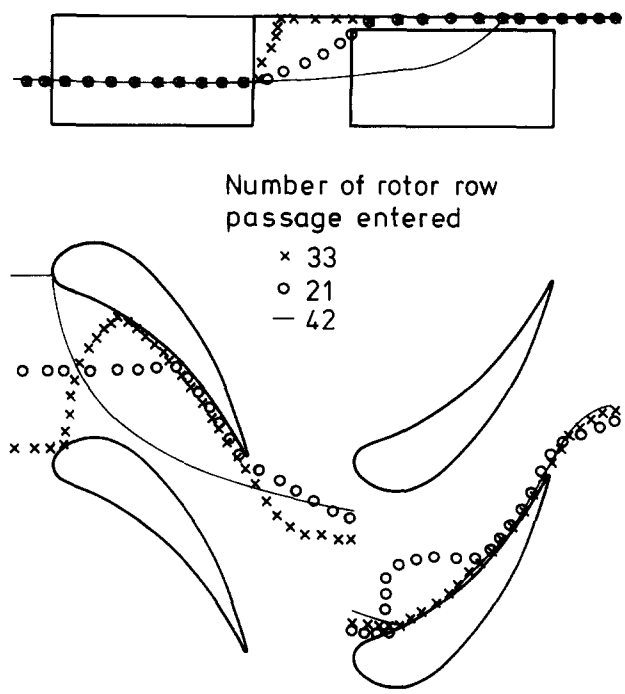

Figure 9 Particle trajectories for nonstandard geometric, flow, and particle properties, $s/s_0 = 0.5$

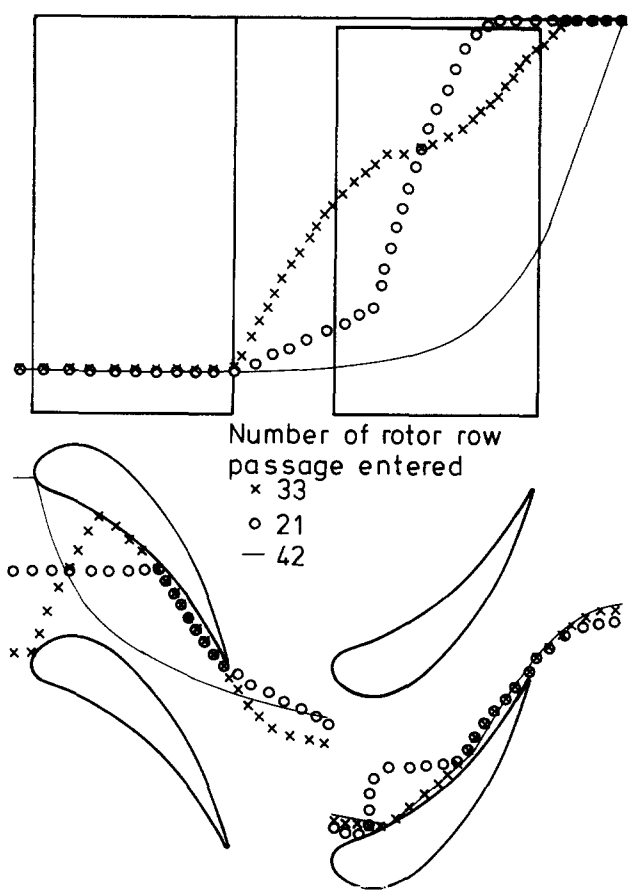

Figure 10 Particle trajectories for nonstandard geometric, flow, and particle properties, $s/s_0 = 2.0$

is, lift is of second-order importance, and for the remainder of this paper, we assumed $E = 0$. Applying Saffman's[22] work on lift to the case illustrated in Figures 7 and 8 is not strictly correct, since it was developed for particles with Reynolds numbers less than unity. In Saffman's case, Reynolds number was based on particle radius, not diameter (as in this work), and, of course, on particle relative velocity. However, the conclusions drawn from Figures 7 and 8 were identical to those found by Kannapprakasam[23] for much smaller particles for which $Re < 1$ was true.

The effects of changes in geometry such as blade span and stator-to-rotor rows spacing are apparent from comparing Figures 9, 10, and 11 with Figures 5 and 6. Increasing row spacing is of marginal significance; it affects the number of the rotor passage entered by a particular particle, which is unimportant if the particle concentration is uniform. This finding is supported by the more extensive data published in Kannapprakasam.[23] Assuming the centripetal accelerations due to the rotor rotation start at the stator trailing edge can have an important bearing on the location of particle impact with rotor blade surfaces when coupled with changes in stator-rotor spacing. Increasing blade span, all other variables remaining unchanged, reduces particle impacts with the casing in the stage, the region and extent of particle impacts with the stator is unaltered, but the number of particle impacts with the rotor pressure surface is increased. Reducing rotor speed means smaller centripetal accelerations in the rotor, and the result of this change is that particles spend a longer period in the rotor passages and have more impacts with the rotor surfaces and, therefore, greater rotor erosion could result (see Figure 12).

The particle density in the standard case is $8000\,kg/m^3$, whereas for the predictions of Figure 13, the particle density is $1112\,kg/m^3$. Comparing Figures 12 and 13 shows that these less dense particles move radially outward in the rotor much more quickly, resulting in many more impacts near the rotor blade leading edge and less farther back. This finding of more rapid radial movement of less dense particles is contrary to expectation. However, these less dense particles make more impacts with stator blade surfaces and, thus, leave the stator passage with low through-flow velocities. Thus these lower density particles have more time to be influenced by centripetal acceleration. The overall effect on erosion of the increased number of impacts may be little changed because of the associated reduced particle densities. This finding on less dense particles is so only if there are many impacts on stator blade

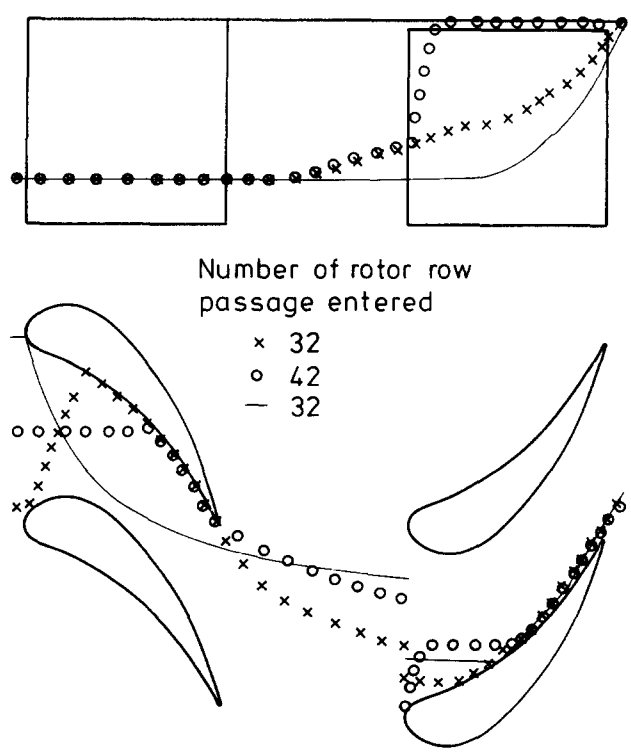

Figure 11 Particle trajectories for nonstandard geometric, flow, and particle properties, $d_{sr}/d_{sr0} = 2.0$

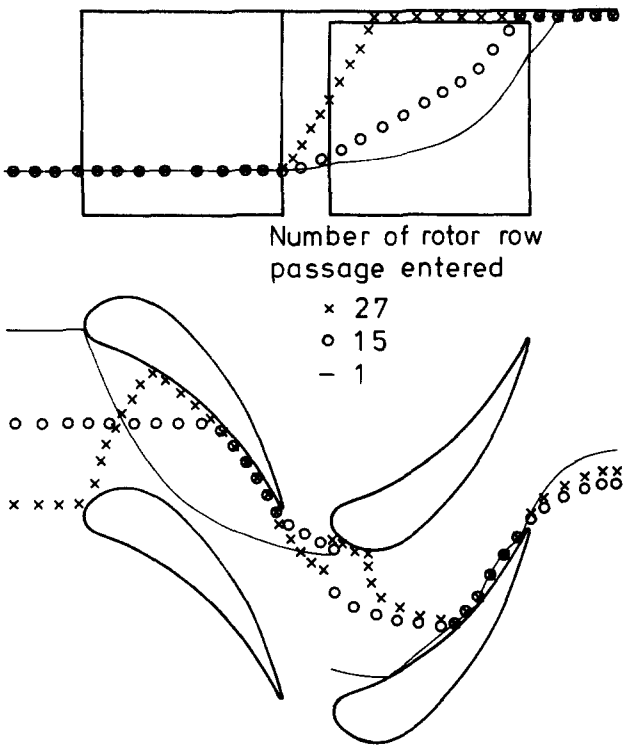

Figure 12 Particle trajectories for nonstandard geometric, flow, and particle properties, $d_{sr}/d_{sr0}=0.5$, $\omega/\omega_0=0.25$

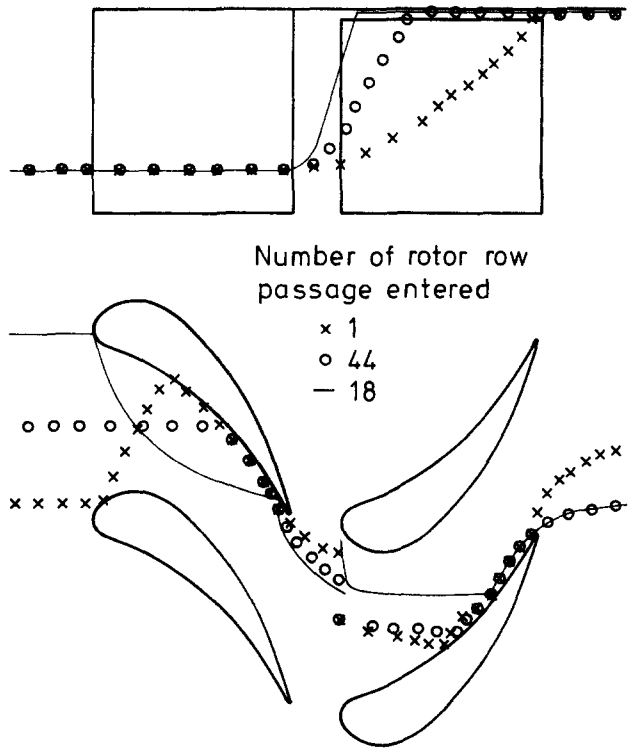

Figure 14 Particle trajectories for nonstandard geometric, flow, and particle properties, $d_{sr}/d_{sr0}=0.5$, $\omega/\omega_0=0.25$, $d/d_0=0.1$

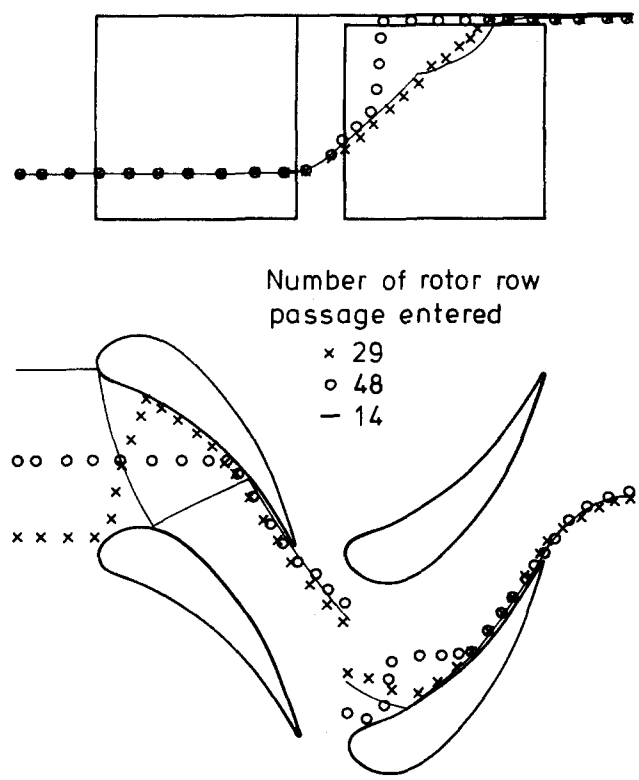

Figure 13 Particle trajectories for nonstandard geometric, flow, and particle properties, $d_{sr}/d_{sr0}=0.5$, $\omega/\omega_0=0.25$, $\rho_p/\rho_{p0}=0.139$

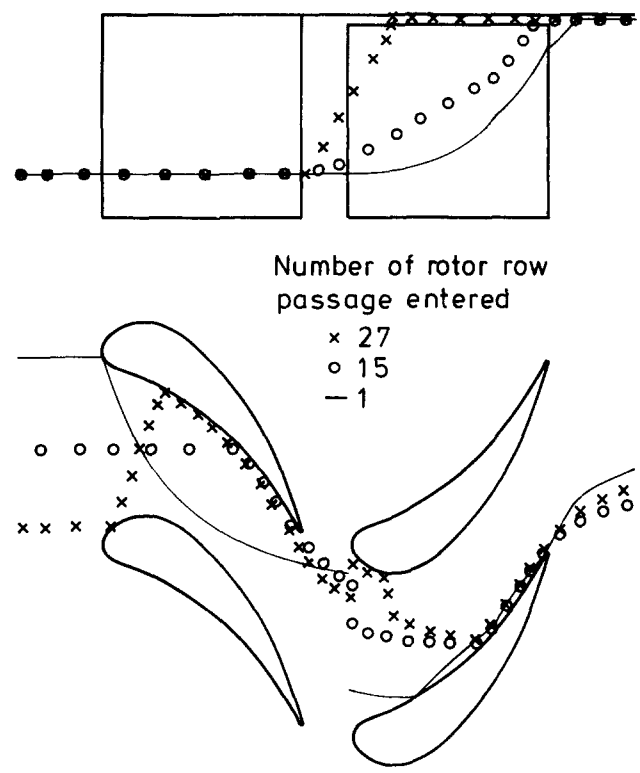

Figure 15 Particle trajectories for nonstandard geometric, flow, and particle properties, $d_{sr}/d_{sr0}=0.5$, $\omega/\omega_0=0.25$, $\psi=0.75$

surfaces. As particle diameter is decreased, the particles follow streamlines more readily, as is apparent from comparing particle trajectories in Figures 13 and 14. The particle trajectory, represented by the continuous line in the stator passage, turns much more rapidly in the case represented in Figure 14 than the corresponding one in Figure 12. This particular particle is also of interest because of its rapid radial movement after leaving the stator passage. The particle had a large incident angle impact with the stator blade pressure surface close to the trailing edge and, by means of Equation 13, has a low velocity when leaving the surface. Thus its trajectory is more influenced by the centripetal acceleration downstream of the stator. These

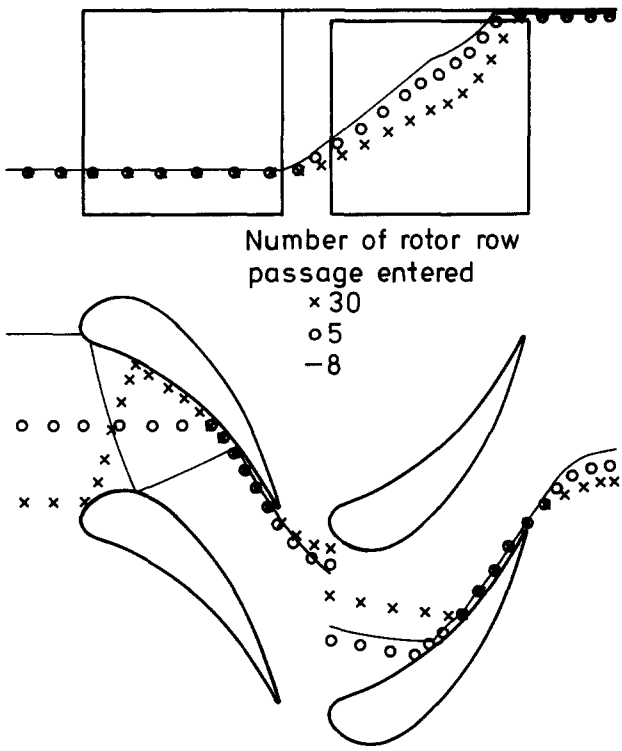

Figure 16 Particle trajectories for nonstandard geometric, flow, and particle properties, $d_{sr}/d_{sr0}=0.5$, $\omega/\omega_0=0.25$, $(V/U)/(V/U)_0=4$

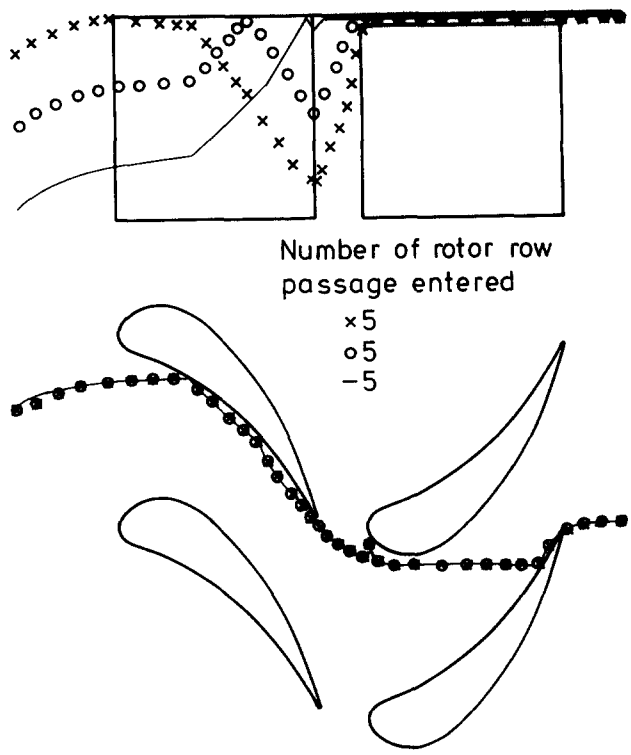

Figure 18 Particle trajectories for nonstandard geometric, flow, and particle properties, $d_{sr}/d_{sr0}=0.5$, $\omega/\omega_0=0.25$, $\theta_b=\theta_c=45°$

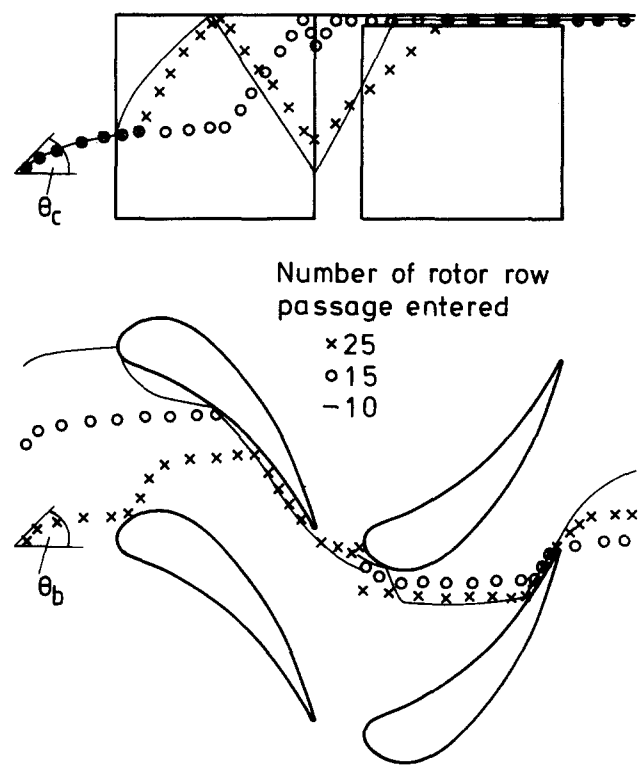

Figure 17 Particle trajectories for nonstandard geometric, flow, and particle properties, $d_{sr}/d_{sr0}=0.5$, $\omega/\omega_0=0.25$, $\theta_b=\theta_c=45°$

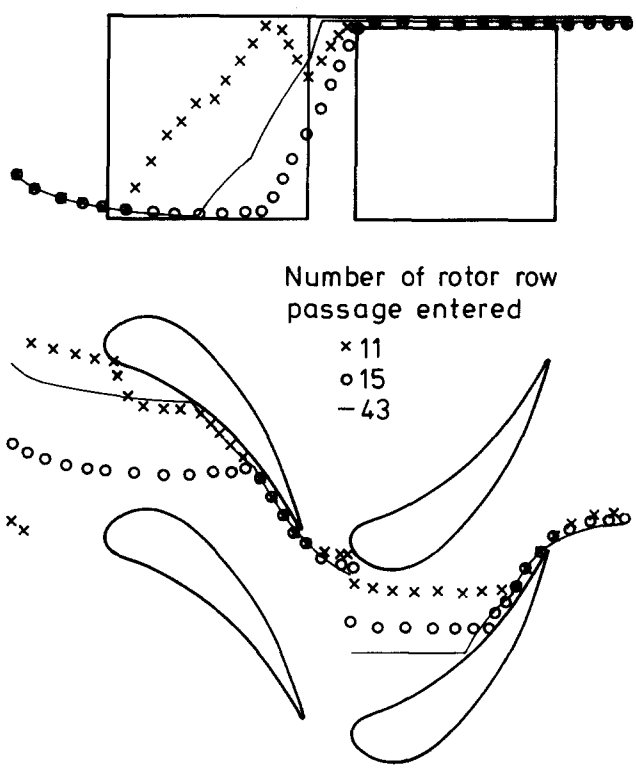

Figure 19 Particle trajectories for nonstandard geometric, flow, and particle properties, $d_{sr}/d_{sr0}=0.5$, $\omega/\omega_0=0.25$, $\theta_b=\theta_c=-45°$

findings on the influence of particle density and diameter on trajectories are in line with those of other workers. Abdel Azim and Rashed[5] stated, "deviation of particle paths from the gas streamlines increased with increased particle mean diameter and material density." The effect of particle angularity on trajectories can be seen by comparing Figure 15 for $\psi=0.75$ with the trajectories of a similar spherical particle shown in Figure 12. The differences in trajectories are small, but even so, the angular particle may cause more erosion because of its shape.

The trajectories of particles of 100 μm diameter or less are more influenced by fluid velocities if their initial velocities are

low (see Figures 16 and 12). The particle represented by the continuous line makes multiple collisions with blade surfaces in the stator passage for $(V/U)/(V/U)_0=4$ compared with the single collision for $(V/U)/(V/U)_0=1$. The particle parameters of importance to their dynamic behavior are their mean diameter, density, and initial velocity.

It has been assumed particles enter a stator passage on a fluid streamline, but this may not be true in practice. The predictions presented in Figures 17 through 20 are for off streamline trajectories at entry to a stage. Clearly, rebound from casing and hub cause more impacts to the stator blades than rebound from streamline entry trajectories. Impacts to rotor blades appear to be confined to the leading edge-tip regions with more impacts to the casing. The predictions presented in Figures 17 through 20 are important, since they are a first step toward suggesting the effect of gross turbulence or vorticity in the free stream on particle trajectories and, therefore, surface erosion in turbines.

In Figures 5 through 20, there is a high concentration of particles close to the stator blade pressure surface in the trailing-

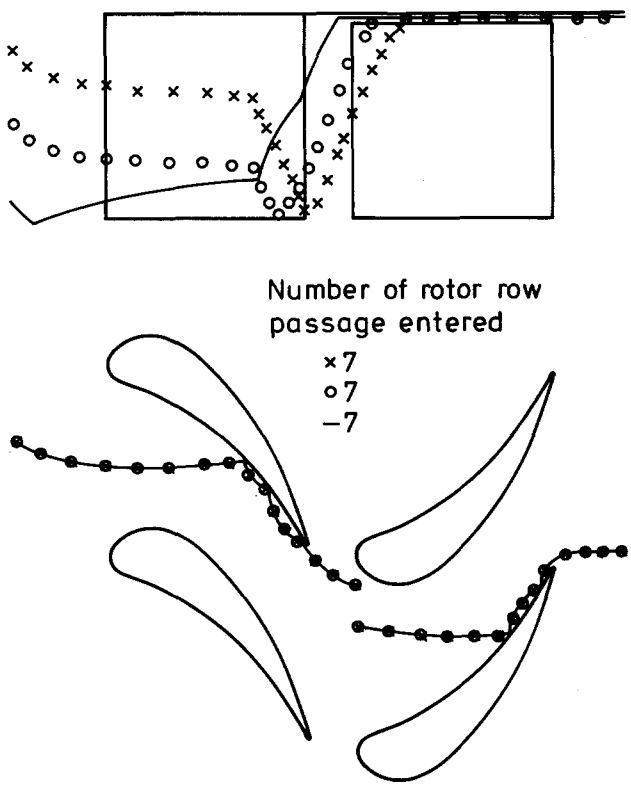

Figure 20 Particle trajectories for nonstandard geometric, flow, and particle properties, $d_{sr}/d_{sr0}=0.5$, $\omega/\omega_0=0.25$, $\theta_b=\theta_c=-45°$

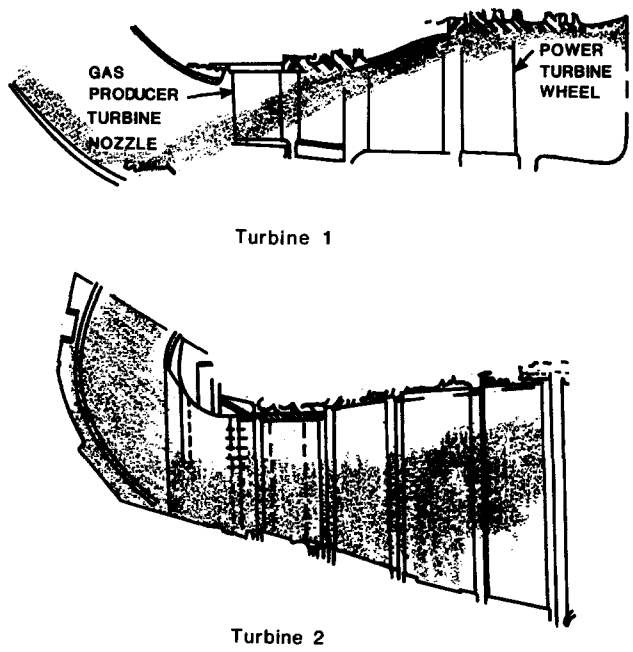

Figure 21 Sand path in two different turbine assemblies (from Connors and Murphy

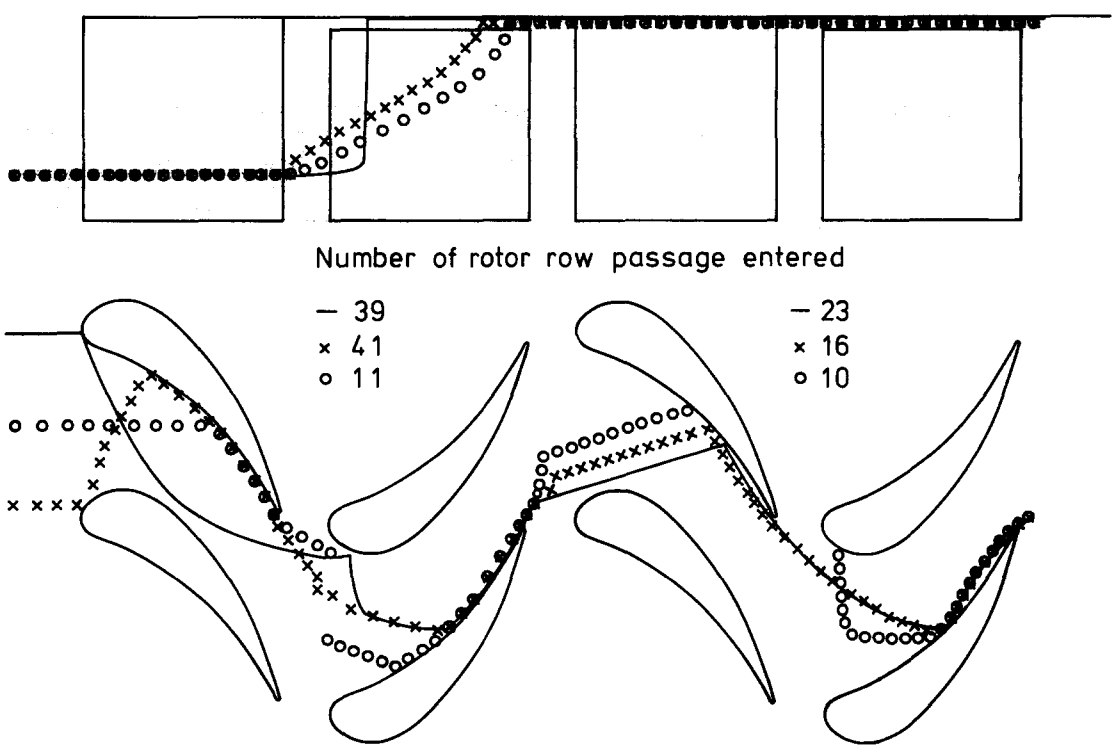

Figure 22 Particle trajectories for two stages with $d_{sr}/d_{sr0}=0.5$, $\omega/\omega_0=0.25$, $(V/U)/(V/U)_0=0.5$

edge region. Thus the subsequent motion of particles will be affected by the stator wake. However, throughout the calculation procedure, the experimentally determined restitution ratios of Grant *et al.*,[6] given in Equations 12 and 13, have been used, which themselves to an extent must take account of stator wake flow.

In examining the predicted particle trajectories, it is worth comparing them with the available experimental evidence, some of which is reproduced from Connors and Murphy[24] in Figure 21. They showed that the first stage was the most prone to erosion and the casing thereafter. The predictions of Figures 5 through 20 basically agree with the findings of Connors and Murphy. However, for completeness, a typical multistage prediction from Kannapprakasam[23] is reproduced in Figure 22, which again compares favorably with the experimental findings of Connors and Murphy. It is difficult to directly compare our predictions with those of other workers because only we have allowed the rotor to start rotating as a particle enters the stator. Moreover, the predictions presented here are from a three-dimensional analysis, whereas other workers' predictions are two dimensional. A direct comparison can be made between the predictions of Tabakoff and Hamed[7] and the authors from Figure 2 and only the stator row of Figures 5 through 16.

Conclusion

Based on the analysis used in the prediction procedure described in this article, we conclude that the three-dimensional dynamic behavior of gas-particle flows can be determined to a level suitable to help in the design of gas turbines. The particle-gas equations have been solved using a fourth-order Runge-Kutta method for each particle, and the gas flow analysis used the streamline curvature method of Katsanis. The procedure included empirical correlations for drag, lift, and rebound, and it has been assumed particle concentrations are low enough to have no significant effect on the gas flow. The lift forces were found to be of second-order importance. The findings on the effect of changing the entry angle of particle trajectory at inlet to a stage are important, since they are a first step toward discovering the relationship between large-scale turbulence and particle impact location.

Serious erosion of gas turbine components can be caused by ingestion of airborne dust, and the anticipated turbine life varies inversely with the product of the maximum particle size and dust concentration.[25] Erosion rate depends heavily on particle impact velocity, and typical correlations relate erosion rate to V^a, where the exponent a lies between 2.3 and 2.9.[26,27] The procedure described in this article can be extended to estimate wear and predict gas turbine component life. This has been done and will be reported in a subsequent article.

Acknowledgements

The authors wish to thank Mrs. S. Thompson, Mrs. P. Jenkins, and Mrs. J. Mosley for their help in preparing the article.

References

1 Morsi, S. A., and Alexander, A. J. Theoretical low-speed particles collision with symmetrical and cambered aerofoils. *ASME*, 1972, paper no. 72WA/FE-35.

2 Lord, M. J., and Singh, U. K. Theoretical study of potential turbine erosion hazard by means of particle trajectory calculations. *Proc. 5th Int. Conf. on Erosion and Liquid Impact*, 1979, Cambridge, 54-1-54-10.

3 Bindon, J. P., and Carmichael, A. D. Streamline curvature analysis of compressible and high Mach number cascade flows. *J. Mech. Eng. Sci.*, 1971, **13**, 344–357.

4 Lord, M. J., and Singh, U. K. Similarity criteria for particle trajectories in geometrically scaled turbine stator cascades. *I. Mech. E. Conf. Gas Borne Particles*, 1981, paper no. C62/81, 11–20.

5 Abdel Azim, A. F., and Rashed, M. I. I. Particle trajectories in a centrifugal compressor. *I. Mech. E. Conf. Gas Borne Particles*, 1981, paper no. C61/81, 1–10.

6 Grant, G., Bell, R., and Tabakoff, W. An approximate study of erosion rebound characteristics of high speed particles impacting a stationary specimen. University of Cincinatti, 1973, tech. rep. no. 73-36.

7 Tabakoff, W., and Hamed, A. Three-dimensional particle trajectories in turbomachinery. *I. Mech. E. Conf. Gas Borne Particle*, 1981, paper no. C63/81, 21–29.

8 Tabakoff, W., and Hussein, M. F. Effects of suspended solid particles on the properties in cascade flow. *AIAA Journal*, 1971, **9**(8), 1514–1519.

9 Tabakoff, W., and Hussein, M. F. Trajectories of particles suspended in fluid flow through cascades. *J. Aircraft*, 1971, **8**, 60–62.

10 Tabakoff, W., Hamed, A., and Hussein, M. K. Investigation of gas-particle flow pressure and solid particle trajectories and velocities in an axial flow cascade pair. *ASME*, 1972, paper no. 72-FT-57.

11 Hussein, M. F., and Tabakoff, W. Calculation of particle trajectories in a stationary two-dimensional cascade. University of Cincinatti, 1972, report no. AD764267.

12 Hussein, M. F., and Tabakoff, W. Dynamic behaviour of solid particles suspended by polluted flow in a turbine stage. *J. Aircraft*, 1973, **10**, 434–440.

13 Hussein, M. F., and Tabakoff, W. Computation and plotting of solid particle flow in rotating cascades. *J. Computers and Fluids*, 1974, **2**, 1–15.

14 Tabakoff, W., and Grant, G. An experimental investigation of certain aerodynamic effects of erosion. *AIAA*, 1974, paper no. 74-639.

15 Tabakoff, W., and Hamed, A. Aerodynamic effects on erosion in turbomachinery. *Joint Gas Turbine Conference, JSME and ASME*, 1977, paper no. 70.

16 Tabakoff, W., and Hamed, A. Erosion study in turbomachinery affected by coal ash particles. *Department of Energy Annual Report*, 1978, contract E(49-18)-2465.

17 Tabakoff, W., and Wakeman, T. Test facility for material erosion at high temperatures. *Erosion: Prevention and Useful Applications*. ASTM STP 664, W. Adler, ed., ASTM, 1979, 123–135.

18 Beacher, B., Tabakoff, W., and Hamed, A. Improved particle trajectory calculations through turbomachinery affected by coal ash particles. *ASME*, 1981, paper no. 81-FT-53.

19 Kannapprakasam, B., and Brown, A. Bases for predicting gas-particle flows with particular reference to turbomachinery. *Int. J. Heat and Fluid Flow*, 1983, **4**(2), 67–77.

20 Katsanis, T. Use of arbitrary quasi-orthogonals for calculating flow distribution in the meridional plane of a centrifugal compressor. NASA TN D2546, 1964.

21 Vanco, M. R. Fortran program for calculating velocities in the meridional plane of a turbomachine, I. centrifugal compressor. NASA TN D6701, 1972.

22 Saffman, P. G. The lift on a small particle in low shear flow. *J. Fluid Mechanics*, 1965, **22**(2), 385–400, and corrigendum, *J. Fluid Mech.*, 1968, **31**, 3, 624.

23 Kannapprakasam, B. Particle flows in gas streams. PhD thesis, University of Wales, 1983.

24 Connors, H. D., and Murphy, J. P. Gas turbine sand and dust effects and protection methods. *S.A.E. Journal*, 1970, no. 700705.

25 Montgomery, E. J., and Clark, E. J., Jr. Dust erosion parameters for a gas turbine. *SAE summer meeting*, Atlantic City, N.J., paper no. 538A, 1962.

26 Sheldon, G. L. Similarities and differences in the erosion behaviour of materials. *J. Basic Eng. Trans., ASME*, 1970, **92**, 619–625.

27 Sheldon, G. L., and Finnie, I. On the ductile behaviour of nominally brittle materials during erosion cutting. *J. Eng. Industry, ASME*, 1966, **88**, 387–392.